MICROCOPY RESOLUTION TEST CHART
NATIONAL BUREAU

AD A116025

MACO/MICRO STUDIES OF HYDROGEN EMBRITTLEMENT MECHANSIMS
IN TITANIUM AND ALUMINUM ALLOYS

FINAL REPORT
for Period October 1976 to October 1981

University of Minnesota
Minneapolis, MN   55455

W. W. Gerberich, P.I.
April 1982

Prepared for
AIR FORCE OFFICE OF SCIENTIFIC RESEARCH
Building 410
Bolling AFB, Washington, C.C.   20332

Under Contract No. AFOSR-77-3133

DTIC
SELECTE
JUN 2 3 1982
H

REPORT DOCUMENTATION PAGE

READ INSTRUCTIONS
BEFORE COMPLETING FORM

1. REPORT NUMBER	2. GOVT ACCESSION NO.	3. RECIPIENT'S CATALOG NUMBER
AFOSR-TR- 82-0508	AD-A116 025	

4. TITLE (and Subtitle)	5. TYPE OF REPORT & PERIOD COVERED
MACO/MICRO STUDIES OF HYDROGEN EMBRITTLEMENT MECHANSIMS IN TITANIUM AND ALUMINUM ALLOYS	FINAL October 76 to October 81
	6. PERFORMING ORG. REPORT NUMBER

7. AUTHOR(s)	8. CONTRACT OR GRANT NUMBER(s)
W. W. Gerberich	AFOSR-77-3133

9. PERFORMING ORGANIZATION NAME AND ADDRESS	10. PROGRAM ELEMENT, PROJECT, TASK AREA & WORK UNIT NUMBERS
University of Minnesota Minneapolis, MN 55455	2306/A1 61102F

11. CONTROLLING OFFICE NAME AND ADDRESS	12. REPORT DATE
AFOSR/NE Bolling AFB, DC 20332	APRIL 1982
	13. NUMBER OF PAGES
	23

14. MONITORING AGENCY NAME & ADDRESS (if different from Controlling Office)	15. SECURITY CLASS. (of this report)
	Unclassified
	15a. DECLASSIFICATION DOWNGRADING SCHEDULE

16. DISTRIBUTION STATEMENT (of this Report)

Approved for public release;
distribution unlimited.

**Approved for public release;
distribution unlimited.**

17. DISTRIBUTION STATEMENT (of the abstract entered in Block 20, if different from Report)

18. SUPPLEMENTARY NOTES

19. KEY WORDS (Continue on reverse side if necessary and identify by block number)

Hydrogen Embrittlement, Titanium Alloys, Aluminum Alloys, Fracture, Fatigue

20. ABSTRACT (Continue on reverse side if necessary and identify by block number)

Systematic studies of environmental effects on fracture in two alpha/beta
titanium alloys, one beta titanium alloy and 7475 aluminum alloys have been
accomplished. Ti-6Al-6V-2Sn has been tested for its hydrogen-induced cracking
behavior under sustained loads. The influence of frequency and microstructure
on fatigue crack growth have also been studied. Fatigue crack growth in Ti-
5Al-4Mo, as a function of hydrogen content, temperature and Widmanstatten colony
size, was then studied. Mechanical data have been obtained along with and

SEM characterizations. Modelling for fatigue thresholds has been attempted to explain dislocation, microstructure and hydrogen effects. Ti-30 Mo has been studied for effects of hydrogen on dislocation dynamics, cleavage fracture stress and fatigue crack propagation. Fractography (SEM) has been used to characterize the fracturing processes and modeling attempted to explain the hydrogen effects. Hydrogen effects in aluminum alloys are not as obvious as those in titanium alloys. Both cathodic and gas-phase charging did not significantly increase the hydrogen content of this material. Mechanical properties did not seem to change decisively after hydrogen charging. But the lack of a macroscopic effect does not preclude a hydrogen mechanism in environmentally assisted events.

I. PROGRAM

Systematic studies of environmental effects on fracture in two α/β-Titanium

alloys, one β-Titanium alloy and 7475 aluminum alloys have been accomplished.

Research programs for each group of material are as follows:

(1) α/β Titanium Alloys

Ti-6Al-6V-2Sn has been tested for its hydrogen-induced cracking behavior

under sustained loads. The influence of frequency and microstructure on fatigue

crack growth have also been studied. Fatigue crack growth in Ti-5Al-4Mo, as

a function of hydrogen content, temperature and Widmanstatten colony size,

was then studied. Mechanical data have been obtained along with TEM and SEM

characterizations. Modelling for fatigue thresholds has been attempted to ex-

plain dislocation, microstructure and hydrogen effects.

(2) β Titanium Alloy

Ti-30 Mo has been studied for effects of hydrogen on dislocation dynamics,

cleavage fracture stress and fatigue crack propagation. Dislocation dynamics

in this β-titanium was studied in terms of its yield stress, work hardening,

strain rate sensitivity, activation volume and activation energy relationships

to cathodic and gas phase hydrogen charging. Hydrogen effects on the cleavage

fracture stress and DBTT were also investigated. Finally, the fatigue-cracking

properties of Ti-30Mo were studied as a function of temperature and hydrogen

content. Throughout this study, as in the previous one for α/β Titanium alloys,

fractography (SEM) has been used to characterize the fracturing processes and

modeling attempted to explain the hydrogen effects.

(3) 7475 (Al-Zn-Mg-Cu) Alloys

Hydrogen effects in aluminum alloys are not as obvious as those in titanium

alloys. Both cathodic and gas-phase charging did not significantly increase the

hydrogen content of this material. Mechanical properties did not seem to change

decisively after hydrogen charging. But the lack of a macroscopic effect does not preclude a hydrogen mechanism in environmentally assisted events.

The 7475 aluminum alloys have been studied for their stress corrosion cracking (SCC) behavior as a function of temperature and impurity (Fe + Si) content. V-K (stress corrosion cracking velocity versus stress intensity) experiments were initially performed in various aqueous environments; but due to the complexity of SCC, these experiments were finally limited to a distilled-water environment. Temperature coefficients (Activation energies) for SCC have been obtained since the V-K diagrams are obtained as a function of temperature.

Since the aim of these studies is to correlate the mechanical aspects of stress corrosion cracking to the metallurgical aspects of these alloys, the second part of this investigation concentrated on TEM and AES (Auger electron spectroscopy) studies. Using thin electropolished films ($\sim$2000Å thick), the microstructure of these alloys, with emphasis on grain boundary chemistry and structure, have been studied by using the TEM and EDX (energy-dispersive x-ray microanalysis). Data have been obtained for grain boundary precipitate size, distribution, shape and chemistry. Furthermore, similar data have been obtained for the grain-boundary region ($\sim$1000Å in width, may include precipitate free zones). Since SCC in the 7475 alloys is intergranular, AES studies also yielded grain boundary information. A specially designed fracture-stage was used to obtain appropriate SCC fracture surfaces for study in the AES (PHI-595). Good correlation was obtained between the EDX data and the AES results.

II. PERSONNEL AND PUBLICATIONS

This AFOSR grant provided total or partial support for 5 graduate students who will all have graduated with a Ph.D. degree by 1983. There are a minimum of 15 papers published (or to be published) in association with research supported by this grant.

A. List of graduate students totally or partially supported on this grant (with graduation year):

1. Neville Moody   M.S. in metallurgy   1977

                          Ph.D. in metallurgy   1981

2. Kumar Jatavallabhula   M.S. in metallurgy   1978

                          Ph.D. in metallurgy   1981

3. Edwin Pow   M.S. in metallurgy   1979

                          Ph.D. in metallurgy   1982

4. Kenneth Peterson   Ph.D. in metallurgy   1983

5. Weikang Yu   Ph.D. in metallurgy   1983

B. List of publications associated with this grant.

1. W. W. Gerberich and N. R. Moody, FRACTURE, 1977, Vol. 2, ICF4, Waterloo, Canada, p. 829.

2. N. R. Moody and W. W. Gerberich, ICM3, Vol. 2, 1979, p. 513.

3. W. W. Gerberich and N. R. Moody, Fatigue Mechanisms, ASTM STP 675, 1979, p. 292.

4. N. R. Moody and W. W. Gerberich, Mat.Sci. and Engng., 41, 1979, p. 271.

5. W. W. Gerberich, N. R. Moody and K. Jatavallabhula, Scripta Met., 14, 1980, p. 113.

6. N. R. Moody and W. W. Gerberich, Metal Science, 14, p. 95 (1980).

7. N. R. Moody and W. W. Gerberich, Met. Trans. A, 11A, p. 973 (1980).

8. W. W. Gerberich, N. R. Moody, C. L. Jensen, C. Hayman and K. Jatavallabhula, Hydrogen in Metals, ASM, 1981, p. 731.

9. W. W. Gerberich, K. Jatavallabhula, K. Peterson and C. L. Jensen, Advances in Fracture Research, Ed. D. Francois, et. al., 1980, p. 989.

10. K. Peterson, J. C. Schwanebeck and W. W. Gerberich, Met. Trans. 9A, p. 1169, 1978.

11. K. Jatavallabhula and W. W. Gerberich, _Fatigue of Engineering Materials and Structures_, Vol 4:2, p. 173, 1981.

12. E. C. Pow, J. C. Schwanebeck and W. W. Gerberich, _Met. Trans._, 9A, 1978, p. 884.

13. E. C. Pow and W. W. Gerberich, _Scripta Met._, 15, p. 55, 1981.

14. E. C. Pow and W. W. Gerberich, "Temperature Coefficients in Stress Corrosion Cracking of 7475 Aluminum Alloys," to be published in _Corrosion_, 1982.

15. E. C. Pow and W. W. Gerberich, "Effects of impurity (Fe + Si) content on stress corrosion cracking behavior and grain boundary chemistry of 7475 aluminum alloys," to be published.

III. RESEARCH HIGHLIGHTS

(1) α/β Titanium Alloys

A. Ti-6Al-6V-2Sn:

Strain-induced hydride precipitation in the α-phase was responsible for fracture under sustained loads in Ti-6Al-6V-2Sn. These hydrides form when the hydrogen concentration in the crack tip stress field reaches the solubility limit. From expressions describing this event, an equation for the effective stress intensity for hydride precipitation was derived. This value differed from the observed threshold due to the influence of the microstructure on fracture. Quantifying this microstructural effect with a modified Dugdale-Barenblatt equation provided a complete description of the fracture process.

A transition in threshold behavior occurred when samples were thin enough for plane stress conditions to exist across 20 percent of the crack front. Under this condition both the stresses and the fracture change across the crack front. The equations for the effective stress intensity and microstructural effect were modified to reflect this change. Very good agreement was observed when predicted thresholds were compared to the experimental values.

The effects of temperature and microstructure on fracture existed from threshold to failure. Fig. 1 and 2 show the effect of temperature on crack growth behavior. When the activation energy of the rate controlling process was determined from crack growth rates versus observed stress intensity, the results were inconsistent with previous studies. From crack growth rate-effective stress intensity curves, the activation energy corresponded to a rate controlling process of hydrogen diffusion through the continuous β matrix.

Ti-6Al-6V-2Sn exhibited accelerated growth rates near failure at a frequency of 0.2 Hz. The acceleration in crack growth rates was due to both cyclic (striations) and static (cleavage) fracture modes occurring simultaneously. The cleavage was the result of hydride precipitation which began at the stress intensity corresponding to the sustained load threshold. The mechanism of hydride precipitation is the same as that for sustained load failure in this alloy.

B. Ti-5Al-4Mo

Unlike Ti-6Al-6V-2Sn, the experimental alloy Ti-5Al-4Mo did not exhibit sustained load cracking below the plane strain fracture toughness value. This was the case even with 1600 ppm hydrogen. Interestingly, no equilibrium hydrides were observed at this concentration. In an alloy such as Ti-8Al-1Mo-1V they occur near 800 ppm. Why the difference in hydride precipitation behavior exists is unknown. It has been suggested that it is due to α_2 precipitation, requiring at least 6 percent aluminum, which leads to α-phase strengthening and more planar slip band formation. Further studies are needed to define this behavior since it is very important for alloy development and application.

Under certain combinations of temperature, grain size, hydrogen concentration and frequency fatigue crack growth rates are accelerated. This may occur in either the near threshold or near failure regimes of growth or in both regimes. Near threshold, the accelerated growth rates result in reduced thresholds

while at higher stress intensities it results in early failure.

Hydrogen accelerated crack growth rates and reduced thresholds in Ti-5Al-4Mo. The accelerated crack growth rates were due to a change in fracture from cleavage through the α grains to fracture along the α/β interface phase. It has been suggested that the interface phase is a hydrogen stabilized or a metastable hydride phase which could provide a preferential fracture path. The presence of an interface phase does not mean a preferential fracture path exists since it was observed in both alloys at all hydrogen concentrations. Fracture may occur along it when the width reaches a certain size as indicated by the results. Further study is needed to determine if this is the case, and if it is, how interface width affects fracture. Questions on the role of hydrogen in the fracture process need to be answered. Does it enter the fracture process only in interface phase formation? If not, it means that hydrogen transport either by dislocation or stress-assisted diffusion must occur. Since the interface phase only forms at elevated temperatures, it would also mean another mechanism is responsible for fracture such as hydride formation or decohesion.

A specific model with regards to the fracture process could not be developed with the fracture mechanism in question. It was possible to develop a model relating fracture strengths to variables known to influence fracture. A model requiring reduced local static stresses for fracture combined with the modified Dugdale-Barenblatt equation provided a good description of observed threshold behavior. It could not account for a number of effects observed at low temperatures. Modelling of this effect waits definition of the fracture process.

(2) β-Titanium Alloy

A detailed experimental program has been completed to evaluate the effects of hydrogen on dislocation dynamics, cleavage fracture stress and fatigue crack

propagation in Ti-30Mo. The results of dislocation dynamics suggest that hydrogen causes both solid solution softening and hardening. At temperatures greater than 150 Kelvin the effect of hydrogen is to decrease the thermal component of the flow stress and the strain rate sensitivity parameter whereas below 150 K the effects are the opposite. It is observed that the softening effects are most severe in the intermediate hydrogen concentration range of 250-650 wt ppm. and the hardening effects are maximum for 1200 ppm wt of hydrogen. This is also suggested by the observed static strain hardening exponents where the maximum in strain hardening exponents occur above 150 K with 250 ppm wt. of hydrogen. The role of hydrogen is to decrease the cleavage fracture stress and elevate the ductile to brittle transition temperature. The cleavage fracture stress is found to decrease more rapidly with hydrogen as introduced electrolytically compared to gas phase charging. At any temperature the effect of hydrogen is to accelerate the fatigue crack propagation rates. Lower fatigue thresholds are obtained with hdyrogen and the fractography demonstrates that deformation and ductile brittle transitions are important in assessing the hydrogen effects on fatigue crack propagation. Figures 3 and 4 illustrate the effects of hydrogen and temperature on fatigue thresholds and DBTT. It is suggested that hydrogen enhances nucleation of double kinks at higher temperatures resulting in solid solution softening. At lower temperatures it is not clearly known whether resistance to double kink motion by hydrogen, hydrogen induced slip mode change ·or a second phase transformation is responsible for hardening effects. The increase in fatigue crack growth rates with hydrogen at higher temperatures is believed to be a direct effect of solid solution softening. At lower temperatures the effects of the ductile to brittle transition appear to be controlling the fatigue crack propagation.

(3) <u>7475 (Al-Zn-Mg-Cu) Aluminum Alloys</u>

The program to study correlations between stress corrosion cracking (SCC) and microstructure of 20 different 7475-type aluminum alloys is almost completed. All data have been gathered and analysis is underway.

Stress corrosion testing for these alloys has been performed at different environments and temperatures. For the T651-tempered materials, aqueous environments decrease the fracture toughness of the material by 60-80%, depending on the temperature of the environment. Cl^-, Br^-, I^- ions tend to accelerate stress corrosion cracking velocity while SO_4^{--} and NO_3^- ions tend to retard stress corrosion cracking velocity when compared to a distilled-water environment. Regardless of the chemical species in the environment, the threshold for stress corrosion cracking, K_{ISCC}, does seem to be constant for a given temperature. Materials in the TMP-temper have increased resistance to stress corrosion cracking, with a decrease in fracture toughness by less than 50% in the worst cases. The impurity (Fe + Si) level of the alloy has a slight effect on the stress corrosion cracking properties of all the 7475 alloys, as illustrated in a typical V-K diagram in Fig. 5. As can be seen in the plot, the purer alloys are actually more prone to SCC than alloys with high Fe and Si impurity contents. It was also concluded that in the plateau region of the V-K diagram, SCC proceeded with an apparent activation energy of 24 KJ/mole for the T651 material and 44 KJ/mole for the TMP material. These apparent activation energy values are deduced from the gradients of a V vs. 1/T plot such as the one shown in Fig. 6.

Metallurgical characterization of the 7475 alloys started with a TEM study of thin foils. Typical microstructures are shown in Figures 7 to 10. Particular attention was paid to the grain boundary areas of these alloys since SCC occurred only along intergranular paths. Both the grain boundary precipitates and the grain boundary region (including the precipitate free zone, if present) have

been analyzed for their chemistries by using the EDX attachment on the STEM. Typical x-ray microanalysis data is shown in Fig. 11. The conclusion is that a purer alloy (Fe + Si) resulted in more Mg being segregated to the grain boundaries (Fig. 12).

Since SCC occurs only along grain boundaries in the 7475 alloys, surface chemical analysis on fracture surfaces due to SCC should also yield grain boundary chemical information. AES (Auger electron spectroscopy) was used for this purpose to augment data from microanalysis along grain boundaries in the STEM. Typical AES data is shown in Fig. 13, with derived grain boundary information shown in Fig. 14. The Auger data agree qualitatively and well with the EDX data because it also shows that smaller (Fe + Si) contents mean a higher Mg concentration at the grain boundary.

Correlation between the metallurgical results to the mechanical results shows that a purer (less Fe + Si) T651 alloy has a slightly reduced SCC resistance probably due to reduced Mg concentration at the grain boundary. Materials in the TMP temper show a reversed relationship. On the other hand, a purer alloy produces a significant increase in the fracture toughness which far outweighs the slight decrease in SCC resistance. Our experiments did not preclude a hydrogen mechanism in SCC even though hydrogen charging did not produce obvious effects on mechanical properties of these alloys. It is known that Mg forms a Mg-H complex with hydrogen; further studies on the Mg-H complex and grain boundary relationships are needed to further understand the SCC mechanisms.

IV. CONCLUSIONS

(1) Strain-induced hydride precipitation in the α-phase is responsible for static and fatigue fracture in Ti-6Al-6V-2Sn, but not in Ti-5Al-4Mo.

(2) In Ti-30MO (β-titanium), hydrogen causes both solid solution softening and hardening, depending on temperature. Hydrogen accelerates fatigue crack propagation at all temperatures.

(3) A decrease in impurity (Fe + Si) levels in 7475 results in a slight decrease in SCC resistance for the T651 temper. Grain boundary studies show that less Fe + Si in the bulk results in higher Mg concentration at the grain boundaries.
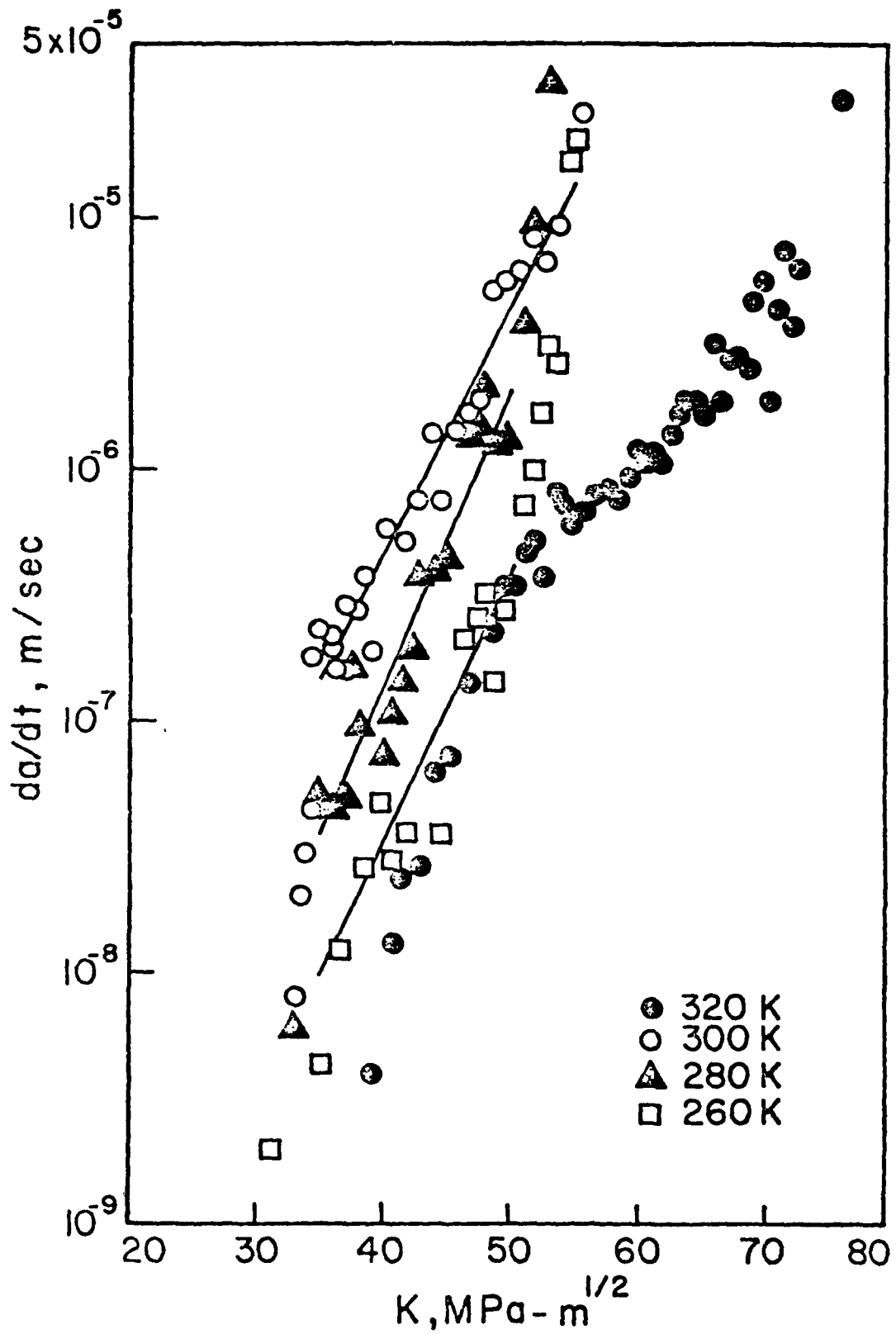
Figure 1. The effect of stress intensity on hydrogen-induced crack growth as a function of T for Ti-6Al-6V-2Sn
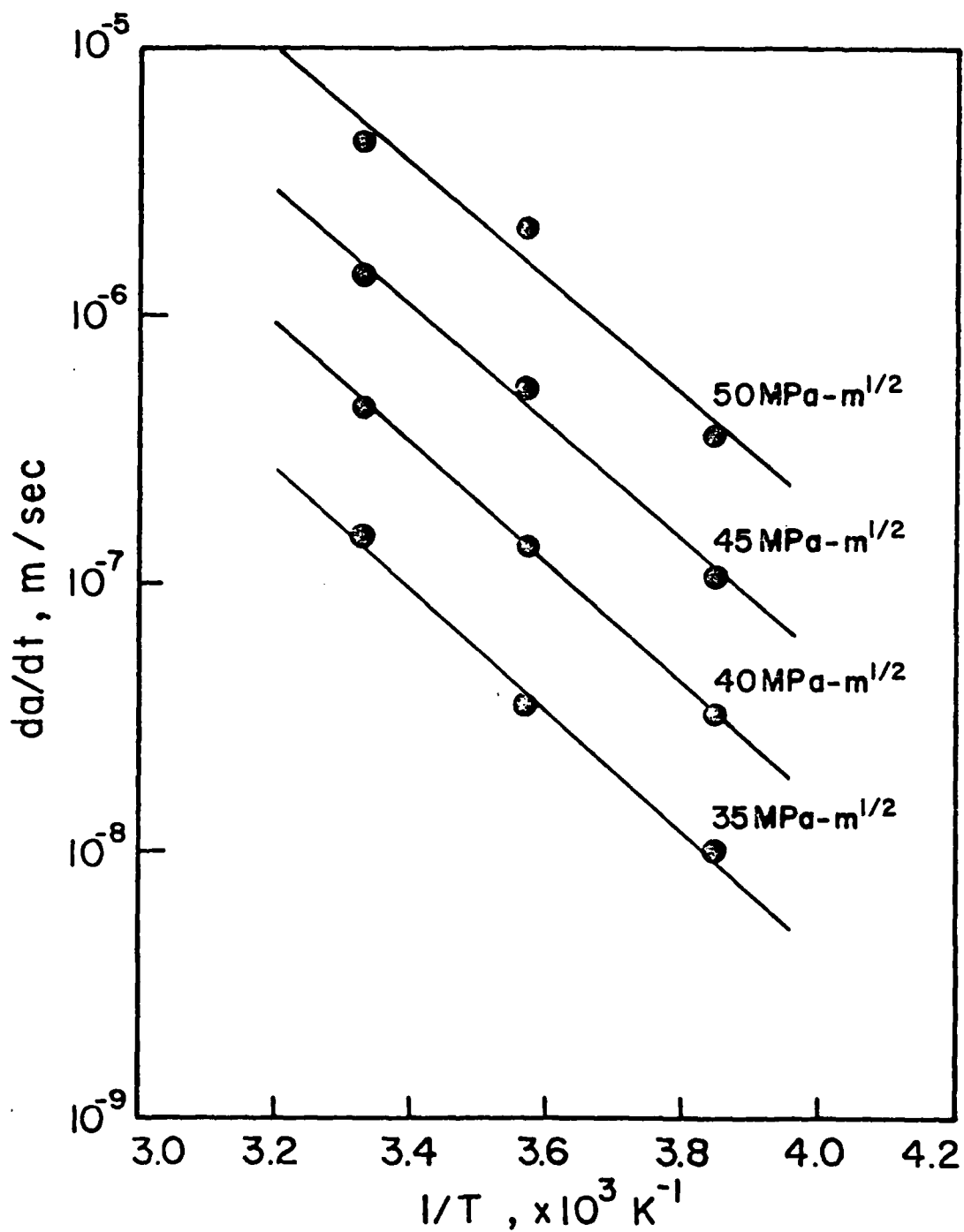
Figure 2. The effect of temperature on crack growth rates exhibiting region IIa(internal hydrogen induced crack growth) behavior as a function of applied stress intensity.
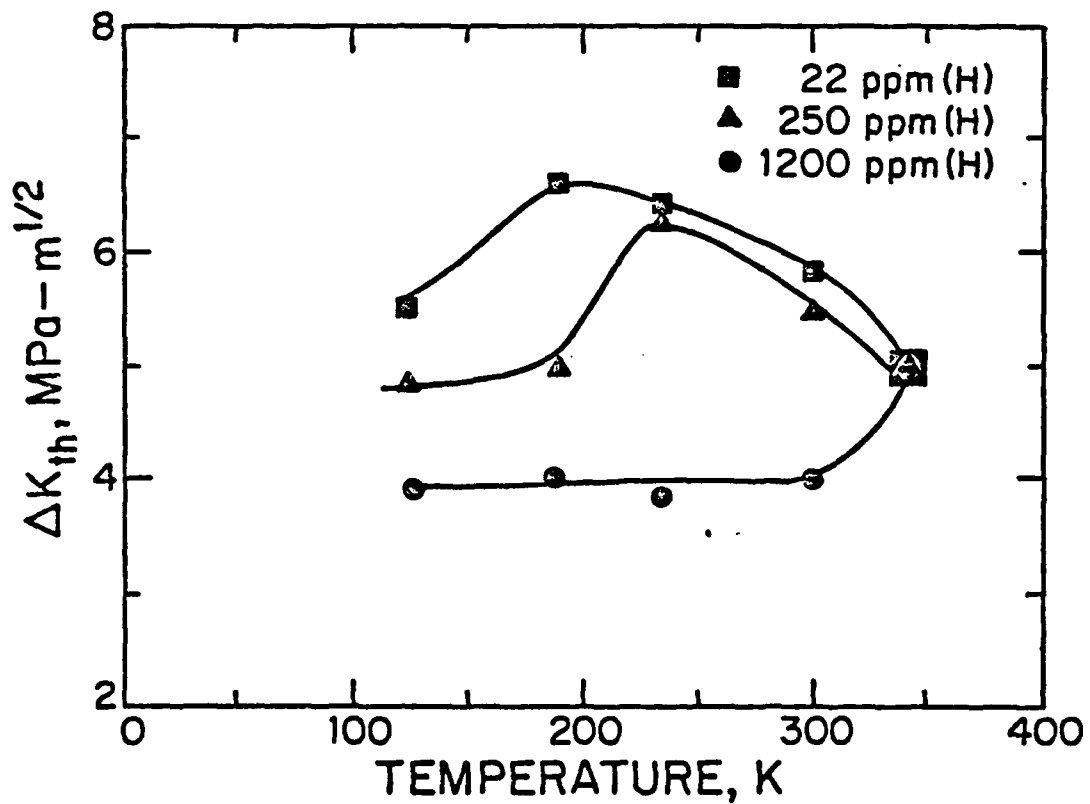
Figure 3. Influence of test temperature on fatigue
thresholds for 22, 250 and 1200 ppm wt
of hydrogen.
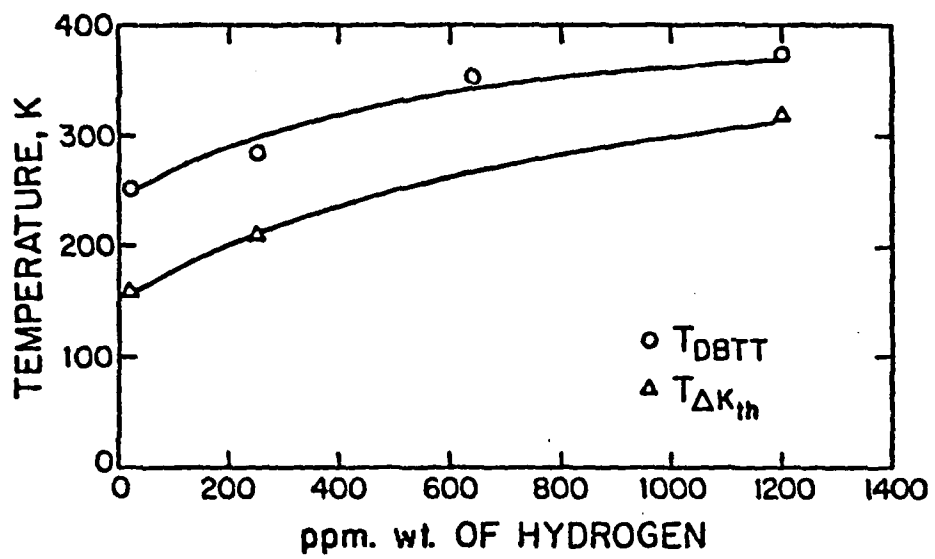
Figure 4. Comparison of the influence of hydrogen on
experimentally observed ductile-brittle
and fatigue threshold transitions.

EFFECT OF (Fe + Si) ON V-K$_I$ CURVE

T651 7475 Aluminum alloy
S-T orientation
60 degree C
Distilled water
Constant Immersion
2000 hr. K$_{ISCC}$

■ 34T651   .02Fe + .01Si
▲ 41T651   .08Fe + .04Si
● 28T651   .20Fe + .11Si

STRESS CORROSION CRACKING VELOCITY   (mm/day)

K$_I$ (MPa·m$^{1/2}$)

Figure 5.

TEMPERATURE COEFFICIENTS(QUASI-ACTIVATION ENERGIES)
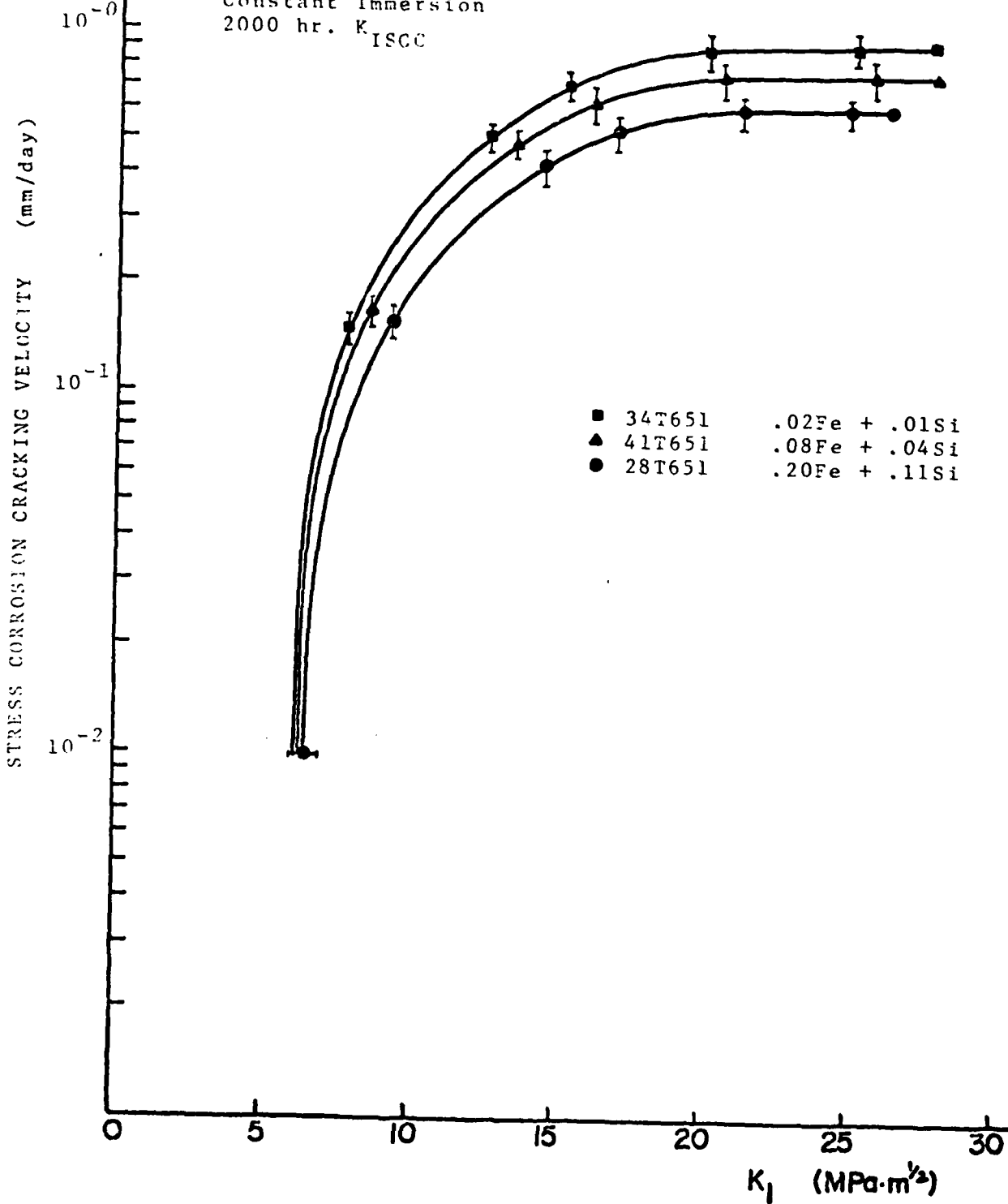
PLOT OF REGION II STRESS CORROSION CRACK PROPAGATION
VELOCITY VERSUS INVERSE TEST TEMPERATURE

■ 34T651   .02Fe + .01Si
▲ 41T651   .08Fe + .04Si
● 28T651   .20Fe + .11Si

log $V\alpha$ - 1/T

TEST TEMPERATURE
$1/T \times 10^{-3}$
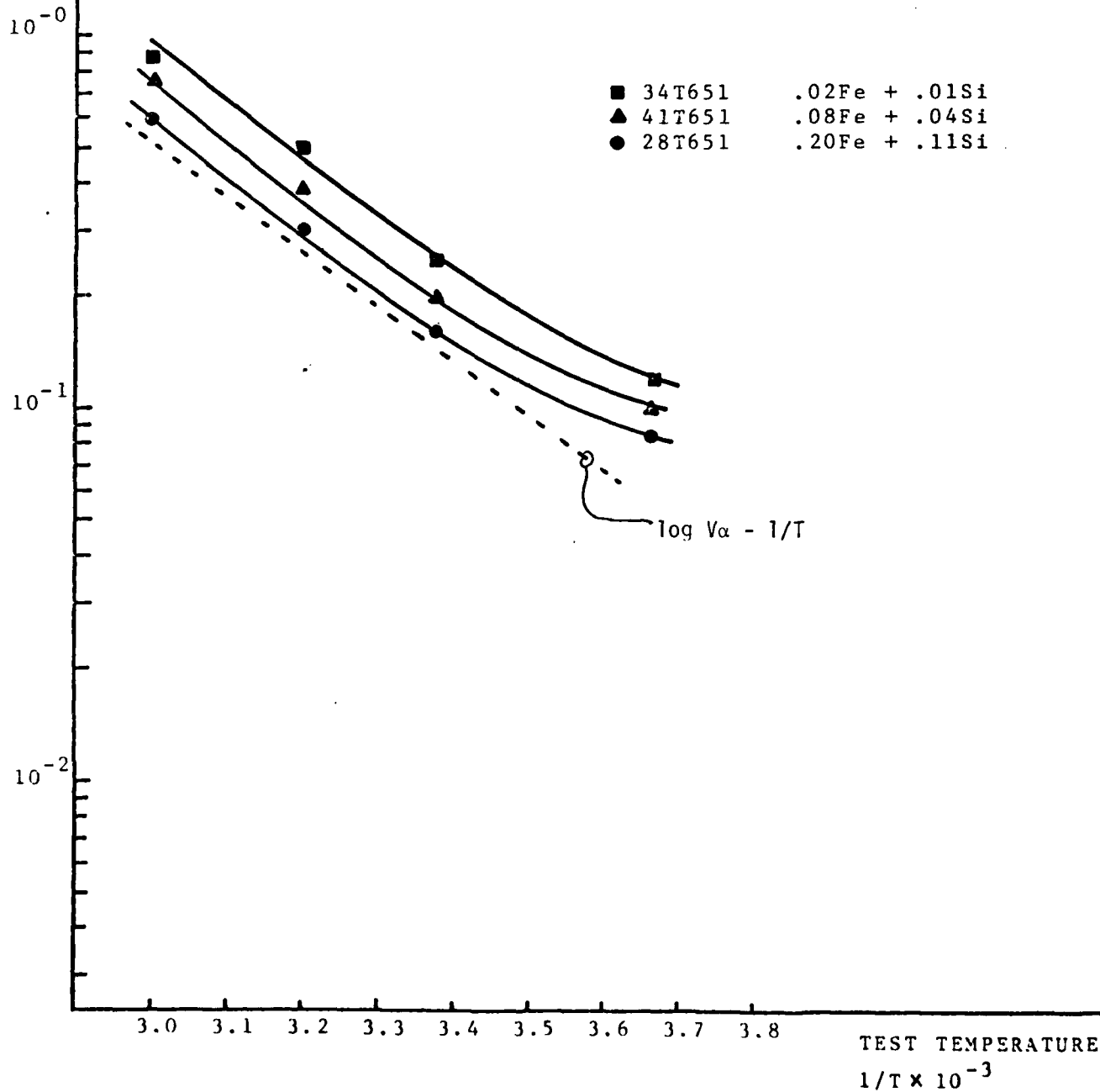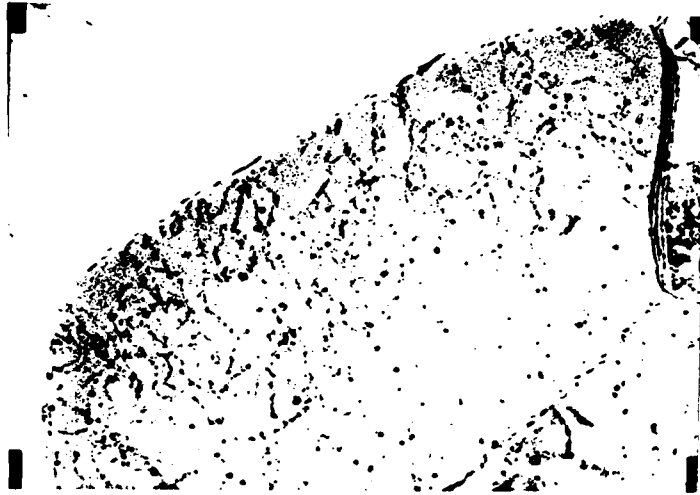
Figure 6

Figure 7   26000X
            Dislocation and precipitate
            relationships within grain.
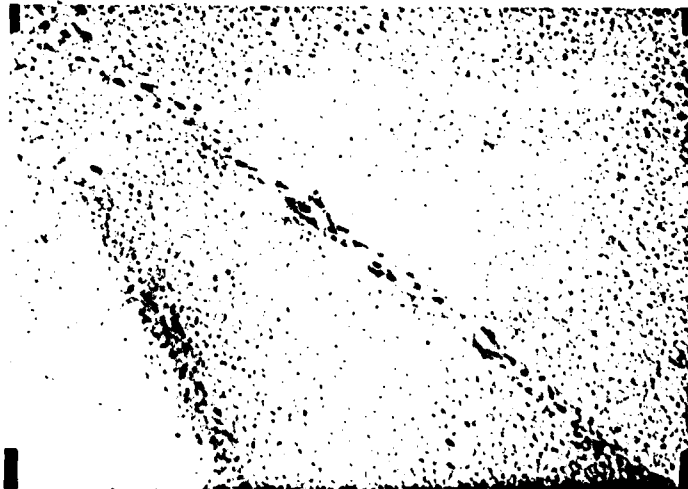
Figure 8   100,000X
   Grain boundary region of
            a T651-temper alloy.
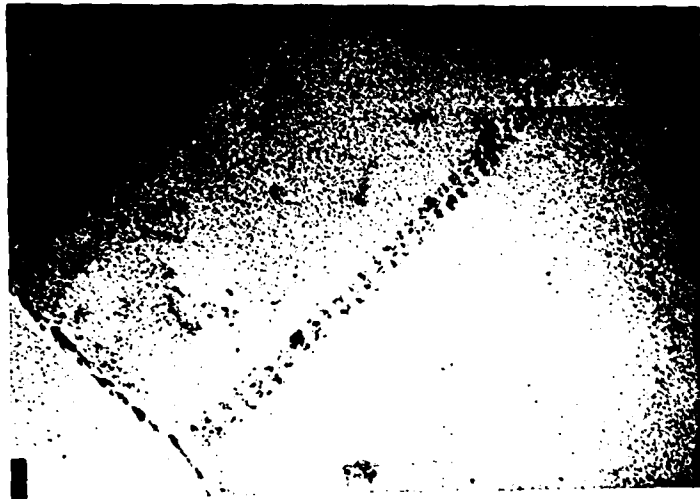
Figure 9   50,000X
            Low angle boundary in a
            T651-temper alloy.
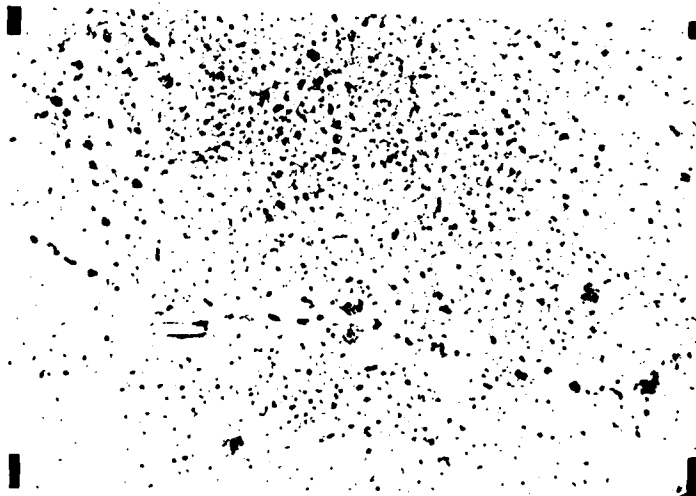
Figure 10   33,000X
            Grain boundary region of
            a TMP-temper alloy.
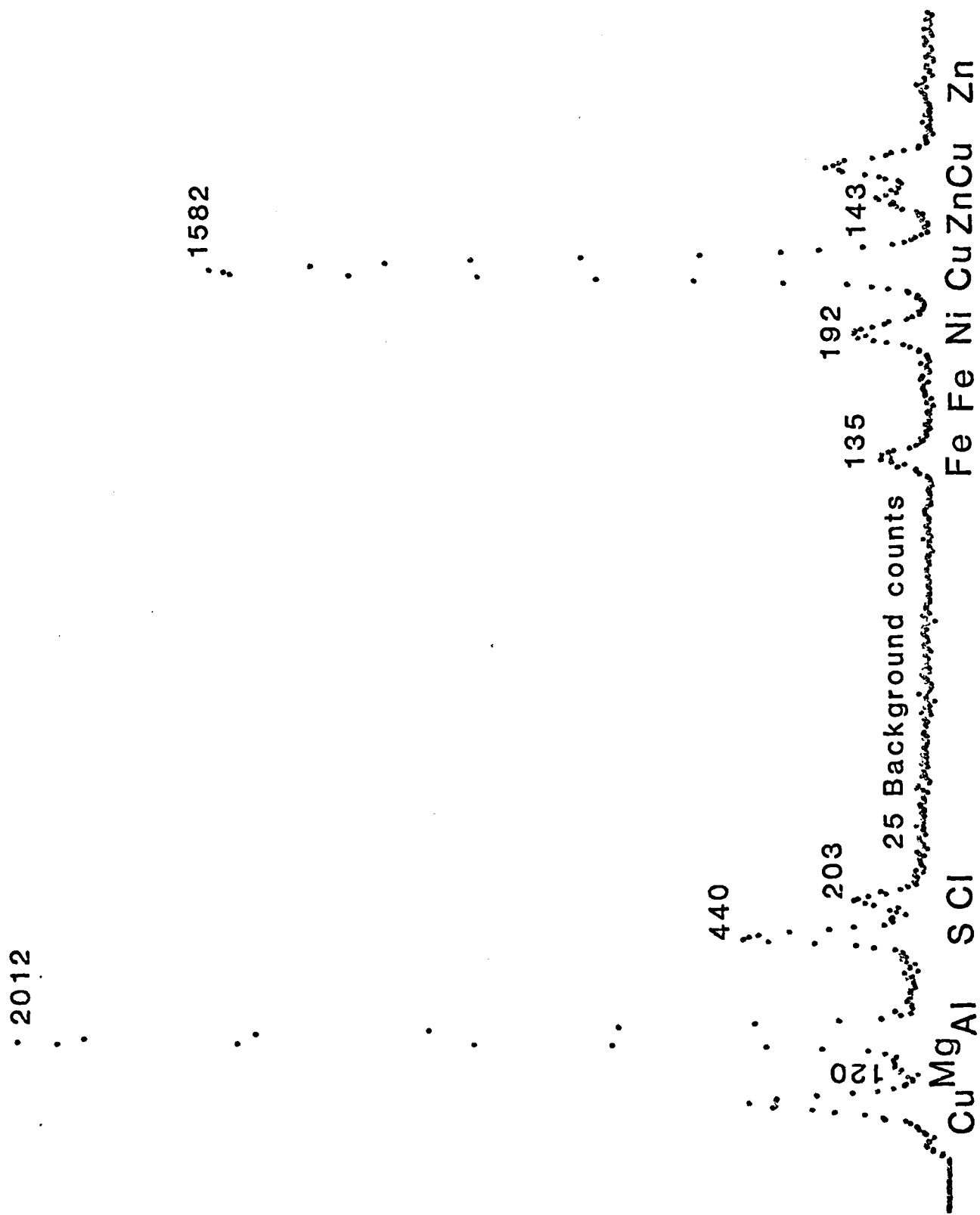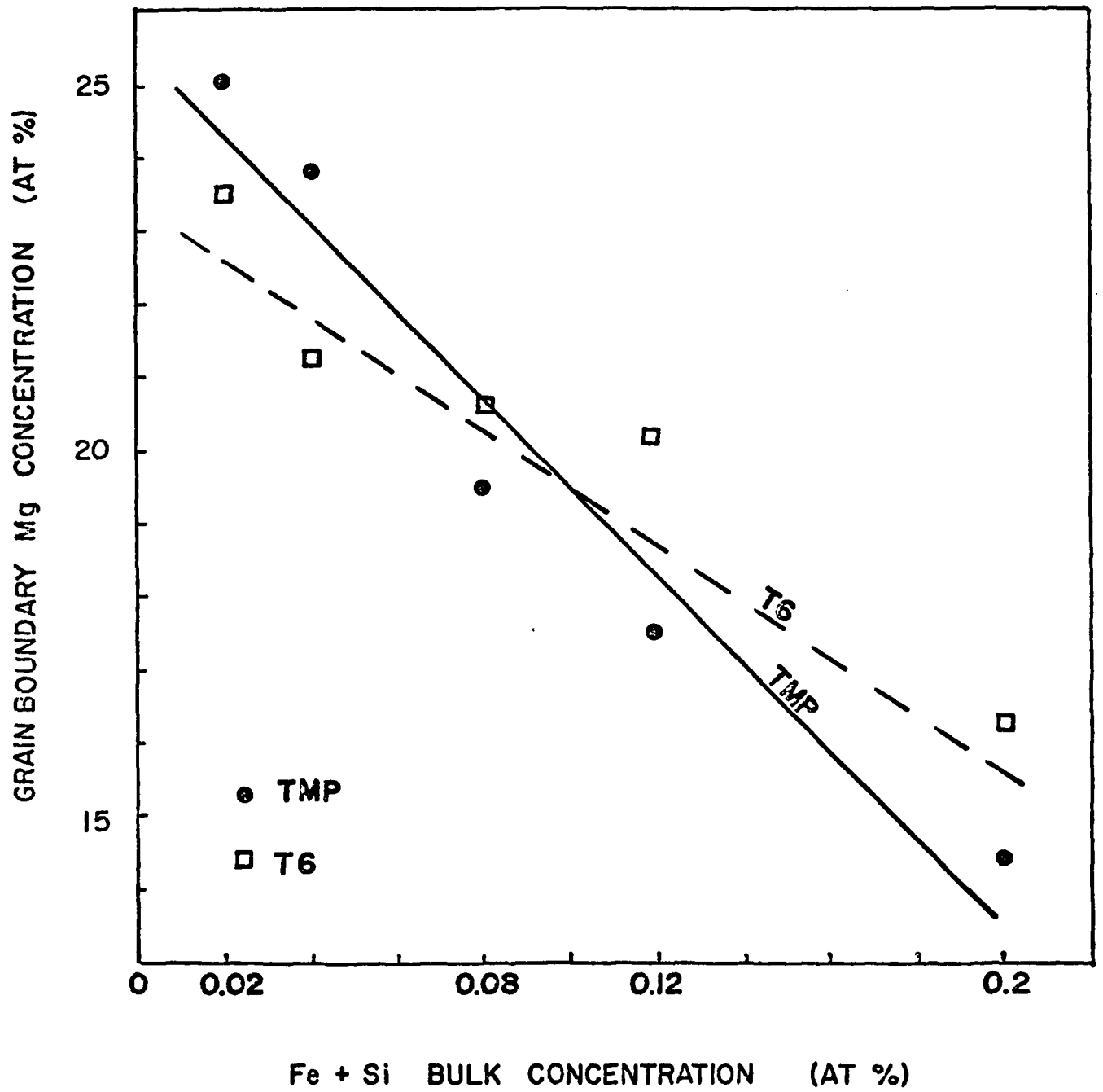
Figure 11.

Figure 12. Plot of grain boundary region Mg content as a
function of bulk content of Fe+Si. (EDX data)
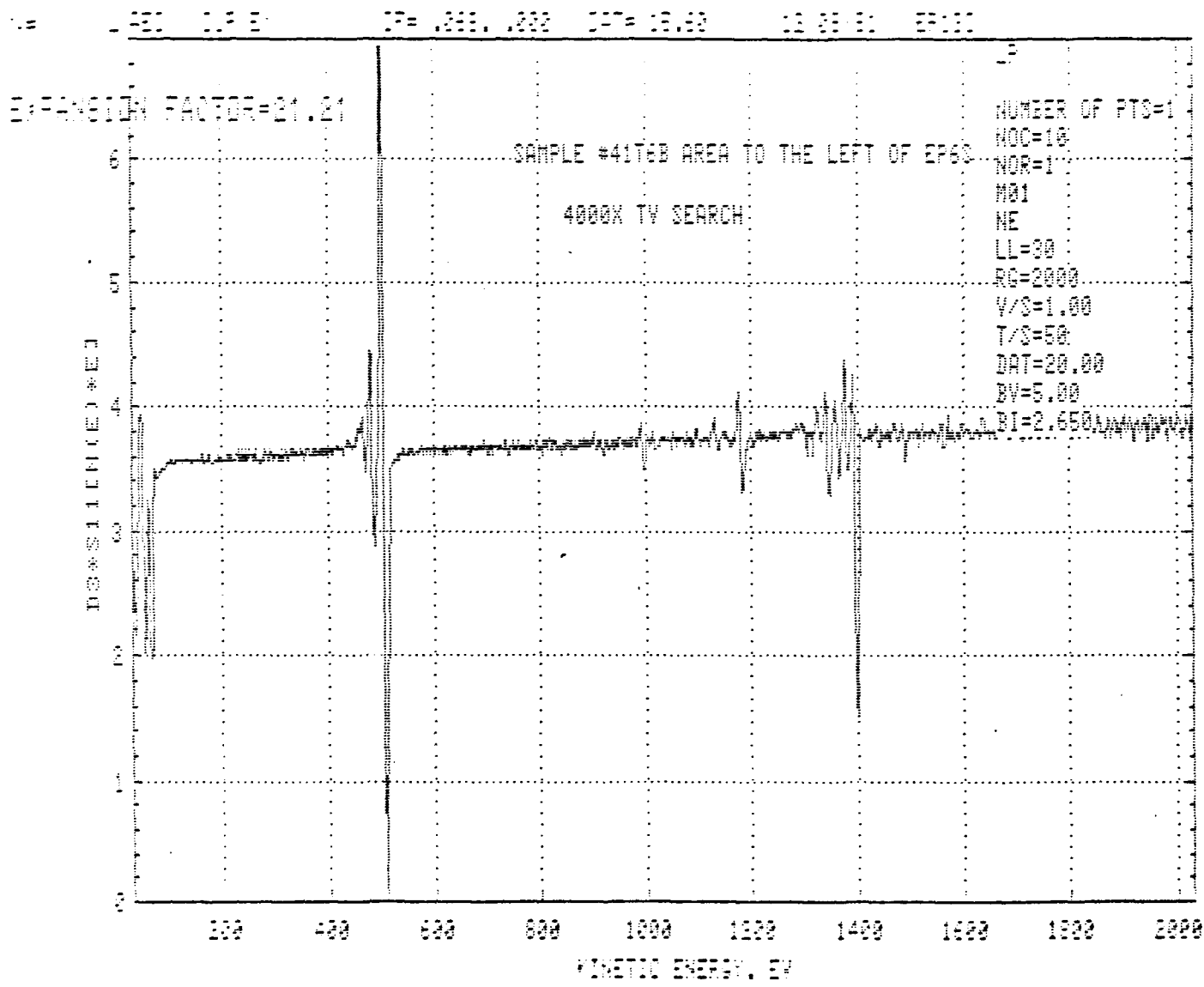
Figure 13. Typical AES data(PHI 595 Scanning Auger Spectrometer)
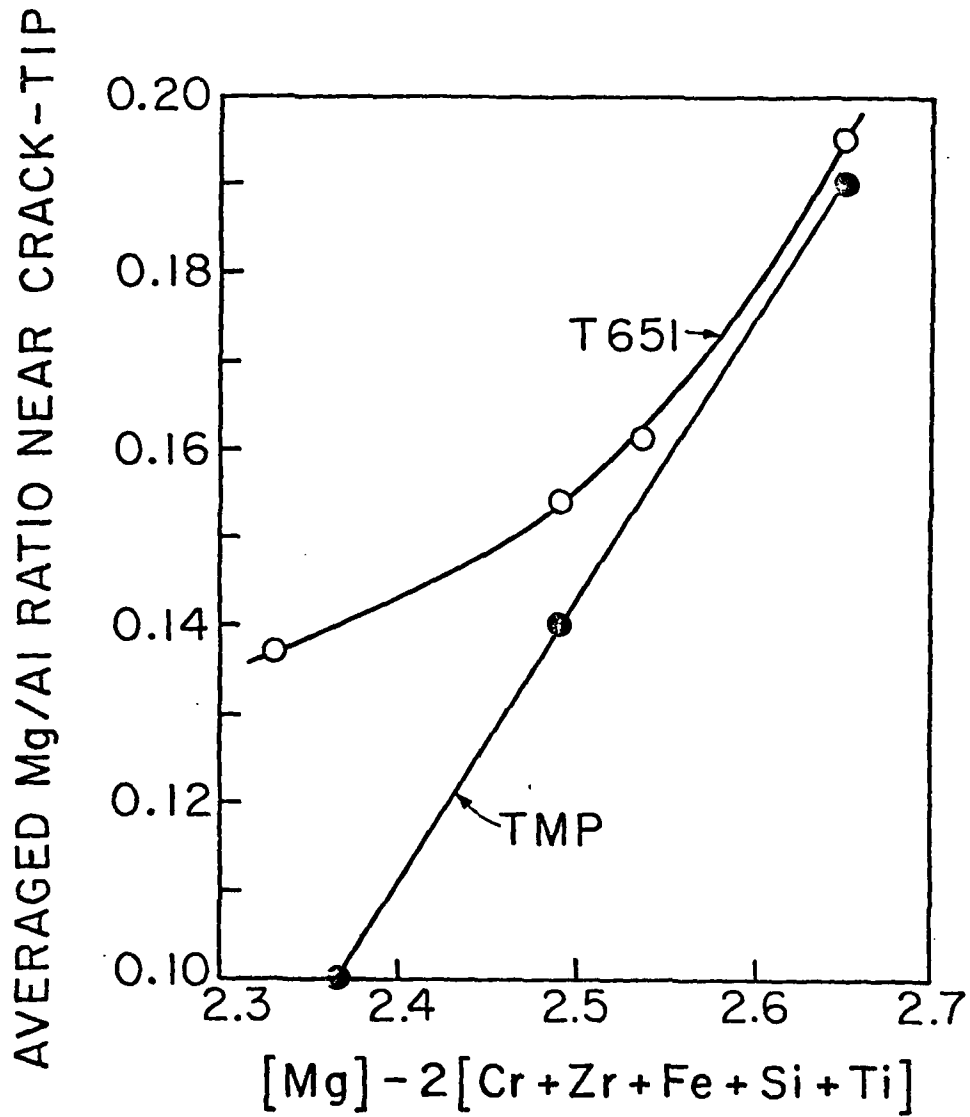
Figure 14. Intergranular fracture surface Mg content as a function of bulk Fe+Si. (Auger data)

END

DATE
FILMED

7-82